Vascular and inflammatory stresses mediate atherosclerosis via RAGE and its ligands in *apoE*$^{-/-}$ mice

Evis Harja,[1] De-xiu Bu,[1] Barry I. Hudson,[1] Jong Sun Chang,[1] Xiaoping Shen,[1] Kellie Hallam,[1] Anastasia Z. Kalea,[1] Yan Lu,[1] Rosa H. Rosario,[1] Sai Oruganti,[1] Zana Nikolla,[1] Dmitri Belov,[1] Evanthia Lalla,[2] Ravichandran Ramasamy,[1] Shi Fang Yan,[1] and Ann Marie Schmidt[1]

[1]Division of Surgical Science, Department of Surgery, and [2]College of Dental Medicine, Columbia University Medical Center, New York, New York, USA.

Endothelial dysfunction is a key triggering event in atherosclerosis. Following the entry of lipoproteins into the vessel wall, their rapid modification results in the generation of advanced glycation endproduct epitopes and subsequent infiltration of inflammatory cells. These inflammatory cells release receptor for advanced glycation endproduct (RAGE) ligands, specifically S100/calgranulins and high-mobility group box 1, which sustain vascular injury. Here, we demonstrate critical roles for RAGE and its ligands in vascular inflammation, endothelial dysfunction, and atherosclerotic plaque development in a mouse model of atherosclerosis, *apoE*$^{-/-}$ mice. Experiments in primary aortic endothelial cells isolated from mice and in cultured human aortic endothelial cells revealed the central role of JNK signaling in transducing the impact of RAGE ligands on inflammation. These data highlight unifying mechanisms whereby endothelial RAGE and its ligands mediate vascular and inflammatory stresses that culminate in atherosclerosis in the vulnerable vessel wall.

Introduction

The metabolic and biochemical milieu generated upon entry of lipid into the vessel wall drives the generation of ligands of the receptor for advanced glycation endproduct (RAGE), including advanced glycation endproducts (AGEs), proinflammatory S100/calgranulins, and high-mobility group box 1 (HMGB1) (1–3). Rapid modification of lipoproteins, including the generation of oxidation and AGE epitopes within LDLs (4), upregulates adhesion molecules, colony-stimulating factors, and chemokines, which ignite vascular stress by stimulating infiltration of monocyte/macrophages and lymphocytes (5–8). Products of these cells, including S100/calgranulins and HMGB1, sustain vascular injury (9, 10). Oxidative stress and inflammation promote further generation of AGEs (11, 12) and thereby sustain cycles of cellular stress.

Initial endothelial dysfunction is a priming event in atherogenesis wherein the endogenous barrier, antiinflammatory, antithrombotic phenotype of the endothelium is transformed into one that contributes to initiation and progression of atherosclerosis. RAGE, expressed in multiple cell types including endothelial cells, transduces the impact of its ligands via signal transduction (1–3, 13). We tested the hypothesis that in the RAGE ligand milieu, RAGE contributes integrally to the pathogenesis of vascular inflammation, endothelial dysfunction, and atherosclerosis in *apoE*$^{-/-}$ mice.

Results

RAGE expression in apoE$^{-/-}$ *mouse aorta*. To establish the role of RAGE in the vasculature of *apoE*$^{-/-}$ mice (14, 15) fed rodent chow, we began by evaluating the time course of RAGE expression in atherosclerosis-prone vasculature. In the aortas of *apoE*$^{-/-}$ mice, a sustained, time-dependent increase in RAGE antigen was detected (Figure 1A). Beginning at age 10 weeks, a statistically significant increase in RAGE expression versus 6 weeks was noted, and by age 24 weeks, an approximately 6-fold increase in expression of RAGE versus 6 weeks was observed ($P < 0.001$; Figure 1A). Of note, at age 24 weeks, RAGE antigen was detected as 2 bands. Previous studies illustrated that RAGE immunoreactivity occasionally revealed more than one band, due either to alternative splicing or to differences in N-glycosylation (16, 17).

To delineate the sites of RAGE expression in the aorta, we performed immunohistochemistry on aortas of *apoE*$^{-/-}$ mice at age 10 weeks. RAGE expression was particularly evident in endothelial cells, as indicated by colocalization with CD31-expressing epitopes (Figure 1, B–D). Controls with nonimmune IgG revealed no specific immunoreactivity (Figure 1E). We performed immunohistochemistry to determine whether RAGE was expressed in smooth muscle cells at this early stage of vascular disease in *apoE*$^{-/-}$ mice. As illustrated in Figure 1, F–H, RAGE was expressed in medial smooth muscle cells, albeit to a lower degree than that observed in endothelial cells.

RAGE impacts atherosclerosis and endothelial function in apoE$^{-/-}$ *mice*. Based on these findings, we sought to dissect the role of the ligand-RAGE interaction in *apoE*$^{-/-}$ mice and used 2 distinct strategies. First, homozygous *RAGE*$^{-/-}$ mice, backcrossed more than 12 generations into C57BL/6, were bred into the *apoE*$^{-/-}$ background to obtain *apoE*$^{-/-}$*RAGE*$^{-/-}$ mice. Second, to probe the role of endothelial RAGE in atherosclerosis, a Tg mouse was prepared to express human dominant-negative RAGE (DN-RAGE) specifically in endothelial cells by the preproendothelin-1 (PPET) promoter (18); these are referred to as *Tg PPET DN-RAGE* mice. Truncation of the cytoplasmic domain of RAGE mutes the impact of ligand-RAGE interaction in vitro and in vivo (1–3, 13). Multiple

Nonstandard abbreviations used: AGE, advanced glycation endproduct; DN-RAGE, dominant-negative RAGE; HMGB1, high-mobility group box 1; MCP-1, monocyte chemoattractant peptide–1; oxLDL, oxidized LDL; PPET, preproendothelin-1; RAGE, receptor for advanced glycation endproduct.

Conflict of interest: A.M. Schmidt receives research support from and is a member of the Scientific Advisory Board of TransTech Pharma Inc.

Citation for this article: *J. Clin. Invest.* **118**:183–194 (2008). doi:10.1172/JCI32703.

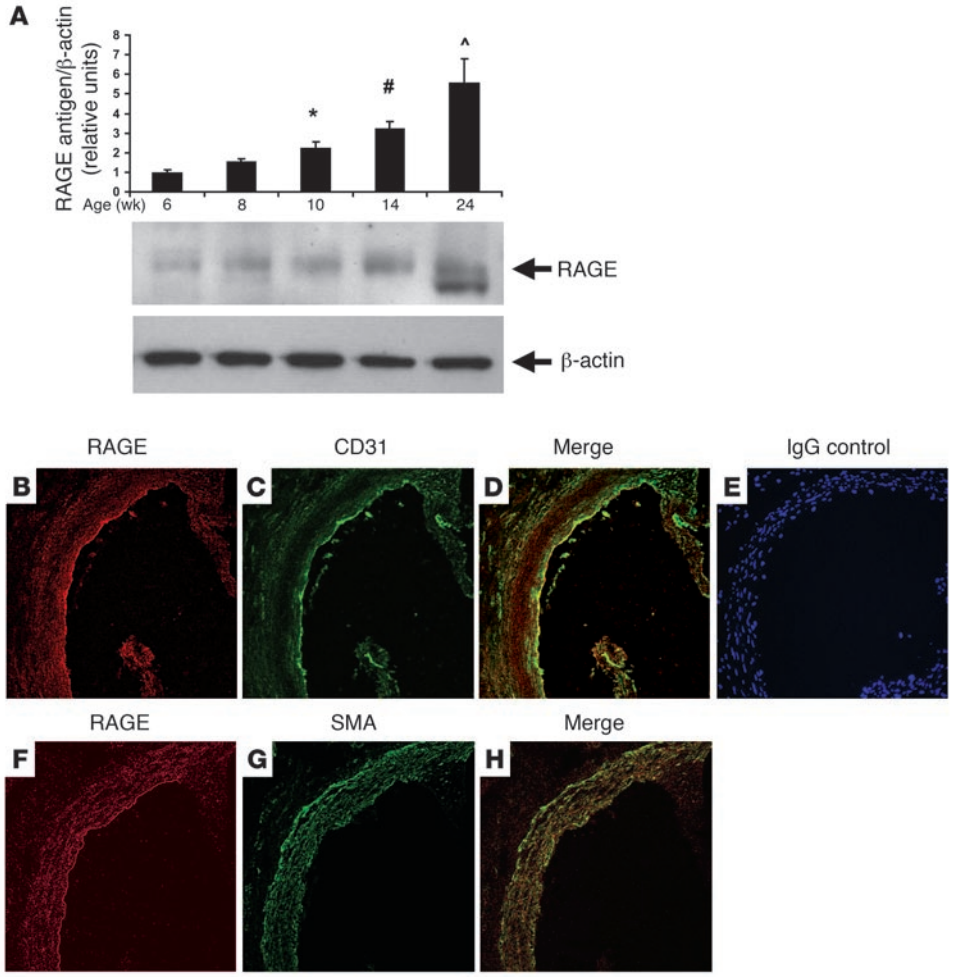

Figure 1
Expression of RAGE in the aortas of *apoE*$^{-/-}$ mice. (**A**) Western blotting. At the indicated ages, aortas were retrieved from *apoE*$^{-/-}$ mice and subjected to Western blotting with anti-RAGE IgG followed by anti–β-actin IgG. RAGE/β-actin antigen relative densitometry units were calculated. $^{*}P = 0.006$, $^{\#}P = 0.0001$, $^{\wedge}P < 0.0001$ versus 6 weeks. (**B**–**H**) Immunohistochemistry. Aorta tissue was subjected to immunohistochemistry to detect RAGE antigen (**B** and **F**). Sites of prominent RAGE expression were confirmed to be endothelial cells, based on colocalization of RAGE expression with CD31 (**C**) in the merged image (**D**). RAGE was also expressed in smooth muscle cells, based on colocalization with smooth muscle actin (**G**) in the merged image (**H**). Staining with nonimmune IgG revealed no specific immunoreactivity (**E**). Original magnification, ×400.

studies in RAGE-expressing cells have revealed the specificity of the DN-RAGE effect to RAGE ligands (2, 13). Specifically, when cells from DN-RAGE mice were incubated with RAGE ligands, abrogation of cellular stimulation was evident. However, when exposed to non-RAGE ligands, such as tumor necrosis factor–α or platelet-derived growth factor, cellular stimulation in DN-RAGE–expressing cells was intact and identical to that observed in WT RAGE-expressing cells (2, 13).

Based on these concepts, we introduced DN-RAGE into endothelial cells and prepared Tg mice. Southern blotting and PCR identified these DN-RAGE–expressing mice (Figure 2, A and B). Western blotting revealed a single band at approximately 55 kDa depicting RAGE antigen in WT mouse aortas; in contrast, aortas of *RAGE*$^{-/-}$ mice revealed no RAGE antigen (Figure 2C). Consistent with expression of WT and truncated RAGE, aortas retrieved from *Tg PPET DN-RAGE* mice revealed 2 bands; the upper band depicted WT RAGE and the lower band the truncated RAGE (Figure 2C).

To further support that the effects observed in atherosclerosis would reflect the contribution of RAGE, we retrieved aorta from WT, *RAGE*$^{-/-}$, and *Tg PPET DN-RAGE* mice and performed real-time quantitative PCR to detect mRNA transcripts for 3 distinct receptors implicated in RAGE ligand interactions: CD36, TLR2, and TLR4 (19, 20). Compared with WT mice, no differences in transcripts for *CD36*, *TLR2*, or *TLR4* were evident in *RAGE*$^{-/-}$ or *Tg PPET DN-RAGE* mice ($n = 4$ per group; $P > 0.05$).

Furthermore, we performed additional experiments to ascertain that *macrophages* from *Tg PPET DN-RAGE* mice were not affected by introduction of DN-RAGE. Thioglycollate-elicited macrophages were retrieved from WT, *RAGE*$^{-/-}$, and *Tg PPET DN-RAGE* mice. As illustrated in Figure 2D, macrophages from both WT and *Tg PPET DN-RAGE* mice displayed intact responses to RAGE ligand S100b as assessed by increased phosphorylation of JNK (Figure 2D). As expected, experiments in *RAGE*$^{-/-}$ macrophages revealed diminished phosphorylation of JNK MAP kinase in response to ligand S100b.

Following their characterization, we assessed the impact of RAGE on atherosclerosis in these 3 groups of *apoE*$^{-/-}$ mice. At age 14 weeks, compared with *apoE*$^{-/-}$ mice, in which mean atherosclerotic lesion area at the aortic sinus was 66,839 ± 6,940 μm^2 (Figure 2, E, H, and K), *apoE*$^{-/-}$*RAGE*$^{-/-}$ mice displayed significantly less atherosclerosis (32,084 ± 3,635 μm^2; $P < 0.0001$; Figure 2, F, I, and K). *apoE*$^{-/-}$*Tg PPET DN-RAGE* mice displayed reduced atherosclerosis (13,909 ± 3,222 μm^2; $P < 0.0001$ versus *apoE*$^{-/-}$; Figure 2, G, J, and K). The complexity of the lesions (21), as defined by the presence of cholesterol clefts, necrosis, calcifications, or fibrous caps, was significantly reduced in *apoE*$^{-/-}$*RAGE*$^{-/-}$ and *apoE*$^{-/-}$*Tg PPET DN-RAGE* compared with *apoE*$^{-/-}$ animals ($P < 0.0001$; Figure 2L). There were no differences in plasma cholesterol or triglyceride in these 3 groups of mice (Table 1).

Based on the significant effects of RAGE on atherosclerosis, we prepared aortic rings from these mice to test whether RAGE affects

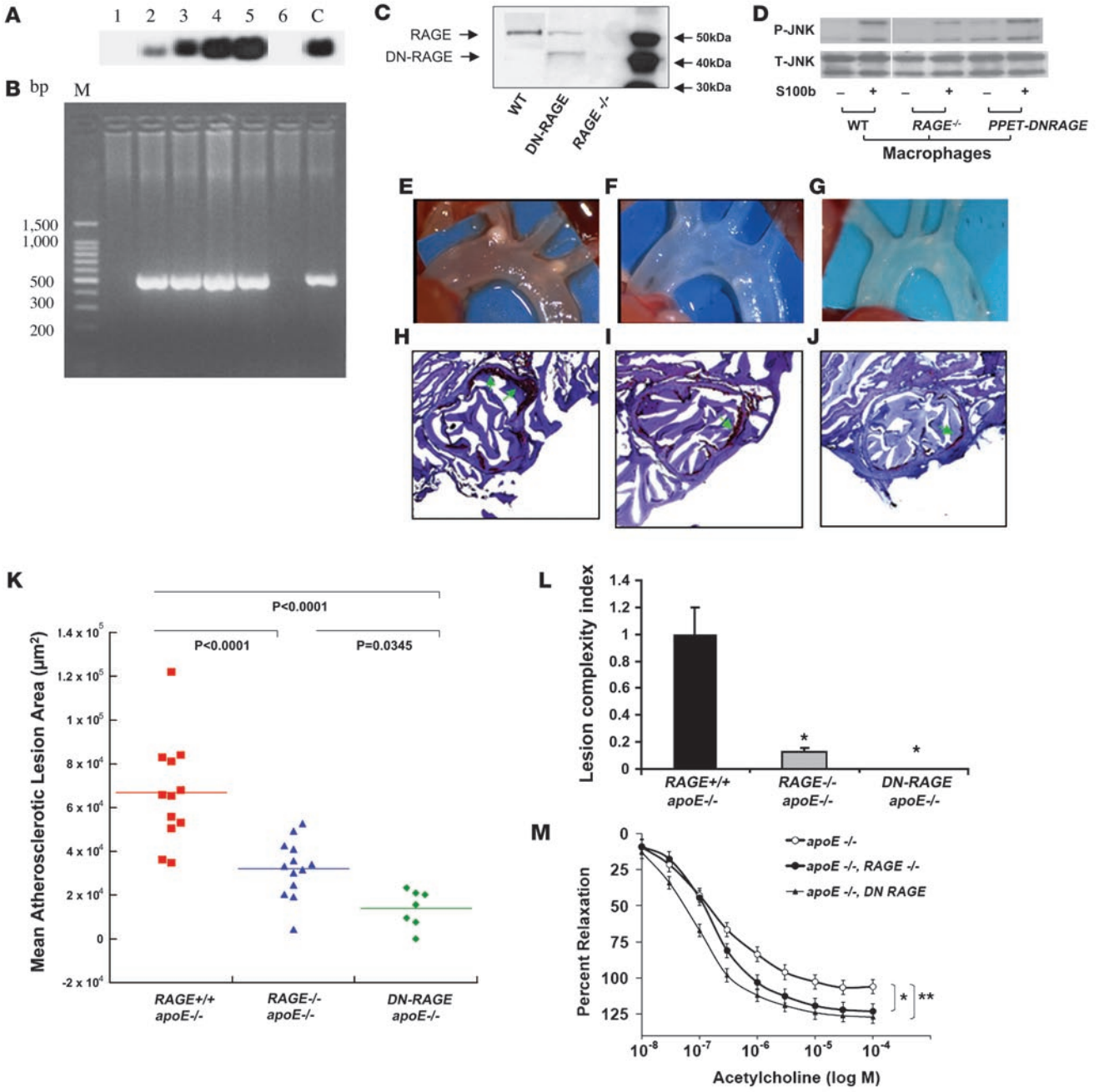

Figure 2

RAGE impacts atherosclerosis and endothelial function in *apoE*$^{-/-}$ mice. Tg mice expressing DN-RAGE in endothelium. Founders were identified by Southern blotting (**A**) and by PCR (**B**). Lanes 1 and 6, lack of PPET DN-RAGE expression; lanes 2–5, expressing PPET DN-RAGE; C, control; M, base pair size marker. (**C**) Aortas were retrieved from the indicated mice and subjected to Western blotting using anti-RAGE IgG. (**D**) Thioglycollate-elicited macrophages were retrieved from the indicated mice and were incubated with S100b for 20 minutes. Western blotting was performed to detect phospho-JNK MAP kinase (P-JNK) followed by total JNK MAP kinase (T-JNK). Where indicated by the white line, lanes were run on the same gel but were noncontiguous. (**E**–**J**) Impact of RAGE on atherosclerosis at 14 weeks. Shown are representative images of aortic arches (**E**–**G**) and sections stained with oil red O (**H**–**J**). (**K** and **L**) Hearts were retrieved from *apoE*$^{-/-}$ (n = 12), *apoE*$^{-/-}$*RAGE*$^{-/-}$ (n = 13), or *apoE*$^{-/-}$*Tg PPET DN-RAGE* (n = 7) mice, and mean atherosclerotic lesion area (**K**) and lesion complexity profile (**L**) were determined. (**M**) Endothelium-dependent vasorelaxation was tested in isolated mouse aortic rings from *apoE*$^{-/-}$, *apoE*$^{-/-}$*RAGE*$^{-/-}$, and *apoE*$^{-/-}$*Tg PPET DN-RAGE* mice (n = 5 per group) sacrificed at 14 weeks of age. Relaxation is reported as percent of initial phenylephrine precontraction. Comparisons were conducted among groups for each agonist dose. *P < 0.05, *apoE*$^{-/-}$*RAGE*$^{-/-}$ versus *apoE*$^{-/-}$ (doses >3 x 10^{-7} M); **P < 0.001, *apoE*$^{-/-}$*Tg PPET DN-RAGE* versus *apoE*$^{-/-}$ (doses >10^{-8} M).

Table 1
Plasma cholesterol and triglyceride in 14-week-old *apoE*$^{-/-}$ mice

Genotype	Cholesterol (mg/dl)	Triglyceride (mg/dl)
apoE$^{-/-}$	248.7 ± 14.1	61.7 ± 7.1
apoE$^{-/-}$*RAGE*$^{-/-}$	223.3 ± 11.9	59.2 ± 7.3
apoE$^{-/-}$*Tg PPET DN-RAGE*	229.1 ± 13.4	57.6 ± 8.2

Deletion of RAGE or endothelial RAGE signaling caused no discernible effect; no significant differences were found between groups.

endothelial-mediated vascular function. Upon exposure of aortic rings to increasing doses of acetylcholine, endothelium-dependent relaxation was significantly enhanced in rings retrieved from *apoE*$^{-/-}$*RAGE*$^{-/-}$ and *apoE*$^{-/-}$*Tg PPET DN-RAGE* mice compared with those of *apoE*$^{-/-}$ mice (Figure 2M).

RAGE impacts vascular inflammation in apoE$^{-/-}$ *mice*. We next focused on central mediators of inflammation and vascular tissue destruction and retrieved thoracic and abdominal aortas of mice at age 14 weeks. Levels of VCAM-1 antigen (5), one of the earliest molecular markers of vascular inflammation in atherogenesis, were significantly reduced in the aortas of *apoE*$^{-/-}$*RAGE*$^{-/-}$ and *apoE*$^{-/-}$*Tg PPET DN-RAGE* mice compared with *apoE*$^{-/-}$ mice (Figure 3A), as were levels of monocyte chemoattractant peptide–1 (MCP-1; Figure 3B) (8). Compared with *apoE*$^{-/-}$ mouse aortas, those of *apoE*$^{-/-}$*RAGE*$^{-/-}$ and *apoE*$^{-/-}$*Tg PPET DN-RAGE* mice revealed significant attenuation in MMP-2 antigen and activity (Figure 3, C and D) (22, 23). Furthermore, compared with *apoE*$^{-/-}$ mouse aortas, those of *apoE*$^{-/-}$*RAGE*$^{-/-}$ or *apoE*$^{-/-}$*Tg PPET DN-RAGE* mice revealed significantly decreased expression of IL-10 and CD40 (Figure 3, E and F) (24–26). To assess the effects of RAGE on expression of its inflammatory ligands, we examined levels of S100/calgranulins and HMGB1 and found that levels of both molecules were significantly attenuated in the aortas retrieved from *apoE*$^{-/-}$*RAGE*$^{-/-}$ and *apoE*$^{-/-}$*Tg PPET DN-RAGE* versus those of *apoE*$^{-/-}$ mice (Figure 3, G and H).

To test that the effects of genetic RAGE modification impacted *systemic* evidence of vascular inflammation, we retrieved plasma from each of the 3 groups of mice at age 14 weeks. Compared with *apoE*$^{-/-}$ mice, plasma retrieved from *apoE*$^{-/-}$*RAGE*$^{-/-}$ or *apoE*$^{-/-}$*Tg PPET DN-RAGE* mice revealed significantly lower levels of soluble VCAM-1 (Figure 3I).

RAGE transduces the effects of S100/calgranulins on vascular inflammation. To specifically dissect the signal transduction mechanisms linking RAGE to endothelial dysfunction, we retrieved and characterized endothelial cells from the aortas of WT C57BL/6 and *RAGE*$^{-/-}$ and *Tg PPET DN-RAGE* mice. Uptake of dil-acetylated LDL and cord formation was observed in these primary murine aortic endothelial cells but not murine fibroblasts (data not shown). By Western blotting, although WT mouse aortas revealed a single band for RAGE antigen at approximately 55 kDa, endothelial cells retrieved from *RAGE*$^{-/-}$ aortas revealed no RAGE-immunoreactive bands (Figure 4A). Endothelial cells from *Tg PPET DN-RAGE* mice revealed 2 immunoreactive bands with anti-RAGE IgG; the higher band indicated full-length RAGE and the lower band the truncated DN-RAGE (Figure 4A).

Based on the observation that RAGE ligand S100/calgranulins was expressed in *apoE*$^{-/-}$ aortas (Figure 3G), we stimulated WT and DN-RAGE endothelial cells with S100b and probed the impact on vascular inflammation and signal transduction cascades. Stimulation of WT endothelial cells with S100b revealed an approximately 5-fold increase in VCAM-1 antigen compared with baseline ($P < 0.0001$; Figure 4B). When endothelial cells were retrieved from *RAGE*$^{-/-}$ or *Tg PPET DN-RAGE* mice, reduced upregulation of VCAM-1 antigen in response to S100b was noted versus stimulated WT endothelial cells ($P < 0.0001$; Figure 4B). When WT endothelial cells were stimulated with S100b, an approximately 8-fold increase in MMP-2 antigen and an approximately 11-fold increase in MMP-2 activity was noted versus baseline ($P < 0.0001$; Figure 4, C and D). However, when endothelial cells were retrieved from *RAGE*$^{-/-}$ and *Tg PPET DN-RAGE* aortas and incubated with S100b, upregulation of MMP-2 antigen and activity was markedly suppressed ($P < 0.0001$; Figure 4, C and D).

We determined the signal transduction mechanisms affected by S100b in aortic endothelial cells. Incubation of WT endothelial cells with S100b induced an approximately 7-fold increase in phosphorylated ERK MAP kinase versus baseline ($P < 0.0001$; Figure 4E). In contrast, when endothelial cells from *RAGE*$^{-/-}$ or *Tg PPET DN-RAGE* mice were incubated with S100b, a highly significant reduction in ERK phosphorylation was observed ($P < 0.0001$ versus S100b-stimulated WT; Figure 4E). When WT endothelial cells were incubated with S100b, an approximately 4.5-fold increase in phospho-JNK MAP kinase was observed versus baseline ($P < 0.0001$; Figure 4F). Key roles for RAGE were illustrated by a significant reduction in S100b-induced phosphorylation of JNK MAP kinase in *RAGE*$^{-/-}$ or *Tg PPET DN-RAGE* endothelial cells ($P < 0.0001$ versus stimulated WT). Of note, S100b failed to upregulate p38 MAP kinase signaling in WT endothelial cells (data not shown).

We next determined which signaling pathway(s) mediated S100b-induced upregulation of VCAM-1 in aortic endothelial cells. WT endothelial cells were incubated with S100b after pretreatment with either PD98059, a MAP kinase inhibitor, or SP600125, an inhibitor of JNK MAP kinases. Although PD98059 had no impact on S100b-induced upregulation of VCAM-1 antigen (Figure 4G), pretreatment of the endothelial cells with SP600125 resulted in highly significant reduction of S100b-mediated VCAM-1 upregulation ($P < 0.0001$; Figure 4H). In addition, introduction of siRNA to knock down JNK expression blunted the effect of S100b on upregulation of VCAM-1 ($P < 0.0001$; Figure 4I). Introduction of scrambled siRNA had no effect on S100b stimulation of mouse endothelial cells (data not shown).

RAGE transduces the effects of oxidized LDL–containing AGEs on vascular inflammation. Previous studies suggested that oxidized LDLs (oxLDLs) contained AGE epitopes (4); thus we probed this concept using affinity-purified anti-AGE IgG and oxLDL, the latter prepared by copper-induced oxidation. Compared with native LDL, Western blotting of oxLDL revealed markedly enhanced AGE immunoreactivity (Figure 5A).

First, we determined whether oxLDL modulates expression of VCAM-1 antigen in WT aortic endothelial cells. Incubation of these cells with oxLDL resulted in an approximately 3.5-fold increase in VCAM-1 antigen by Western blotting ($P < 0.0001$ versus baseline; Figure 5B). When endothelial cells were retrieved from *RAGE*$^{-/-}$ or *Tg PPET DN-RAGE* aortas and incubated with oxLDL, a marked suppression in upregulation of VCAM-1 was noted versus that observed in WT cells ($P < 0.0001$; Figure 5B). Incubation of WT endothelial cells with oxLDL stimulated an approximately 11-fold increase in MMP-2 activity ($P < 0.0001$ versus baseline; Figure 5C). When endothelial cells were retrieved from *RAGE*$^{-/-}$ or *Tg PPET DN-RAGE* mice, a highly significant suppression in oxLDL-

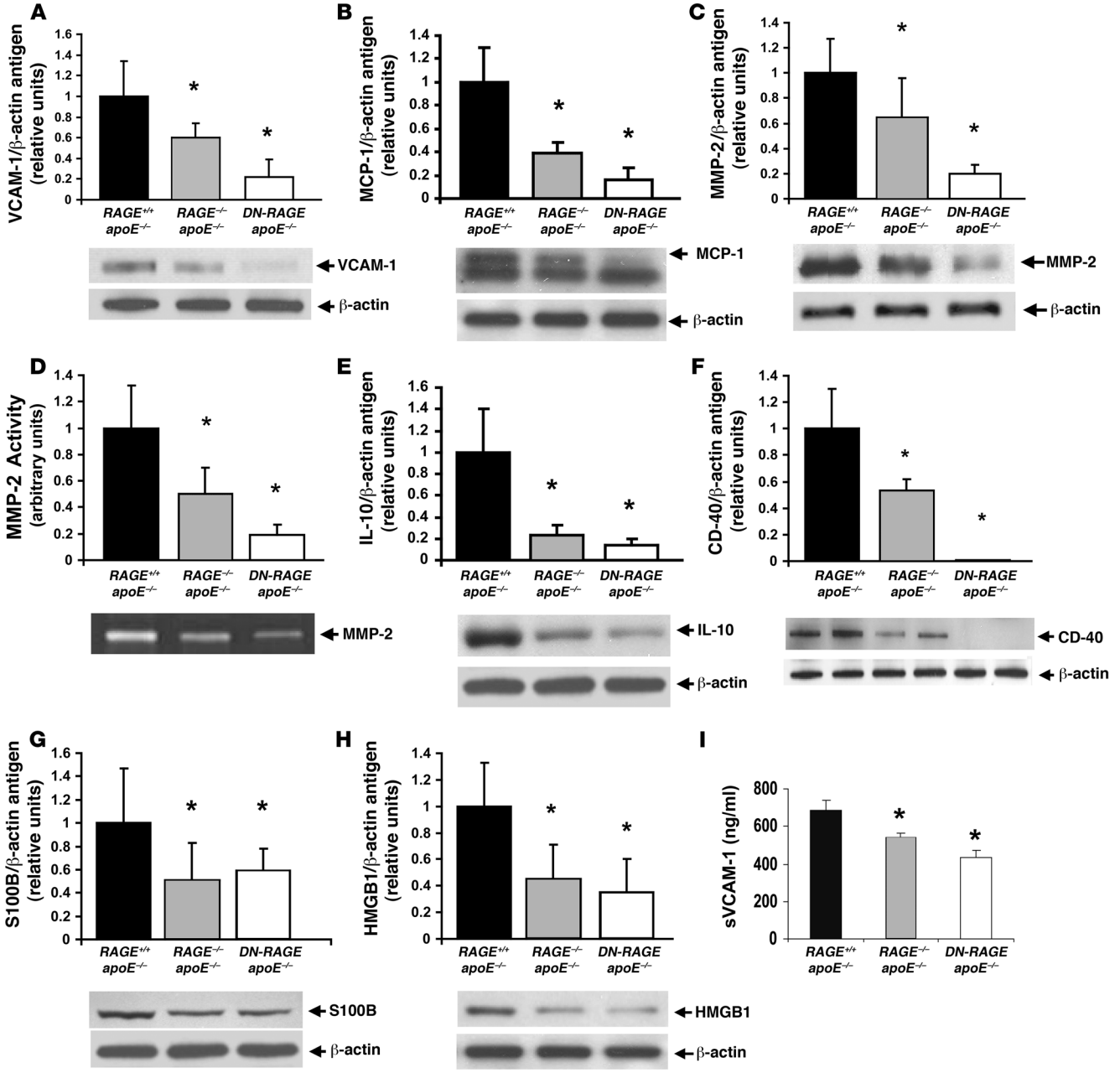

Figure 3

RAGE impacts vascular inflammation in the aortas of *apoE*$^{-/-}$ mice. (**A**–**H**) At age 14 weeks, *apoE*$^{-/-}$, *apoE*$^{-/-}$*RAGE*$^{-/-}$, and *apoE*$^{-/-}$*Tg PPET DN-RAGE* mice were sacrificed and aortas retrieved. Western blotting was performed to detect VCAM-1 (**A**), MCP-1 (**B**), MMP-2 (**C**), IL-10 (**E**), CD40 (**F**), S100b (**G**), and HMGB1 (**H**) followed by anti–β-actin IgG. In **D**, zymography was performed on aorta lysates to detect activity of MMP-2. **P* < 0.001 versus *apoE*$^{-/-}$. (**I**) Plasma was retrieved from 14-week-old mice and subjected to ELISA for determination of soluble VCAM-1 (sVCAM-1) levels. $n \geq 4$ mice per group. **P* < 0.05 versus *apoE*$^{-/-}$.

mediated upregulation of MMP2 activity was noted ($P < 0.0001$ versus WT; Figure 5C).

To test the premise that these oxLDL-mediated changes were evoked by AGE epitopes within oxLDL, we used antibodies to AGE. When WT endothelial cells were pretreated with anti-AGE IgG, significant suppression of oxLDL-induced upregulaton of VCAM-1 antigen and MMP-2 activity was observed compared with nonimmune IgG ($P < 0.0001$; Figure 5, D and E).

To establish the signal transduction pathways mediating the impact of oxLDL-RAGE on upregulation of inflammatory signaling in aortic endothelial cells, we tested the effects on MAP kinases. Incubation of WT endothelial cells with oxLDL induced approximately 4.5- and 2.5-fold increases in phospho-ERK MAP kinase and JNK MAP kinase, respectively, compared with baseline ($P < 0.0001$; Figure 5, F and G). Highly significant reductions in phospho-ERK and JNK MAP kinase were found in *RAGE*$^{-/-}$ and

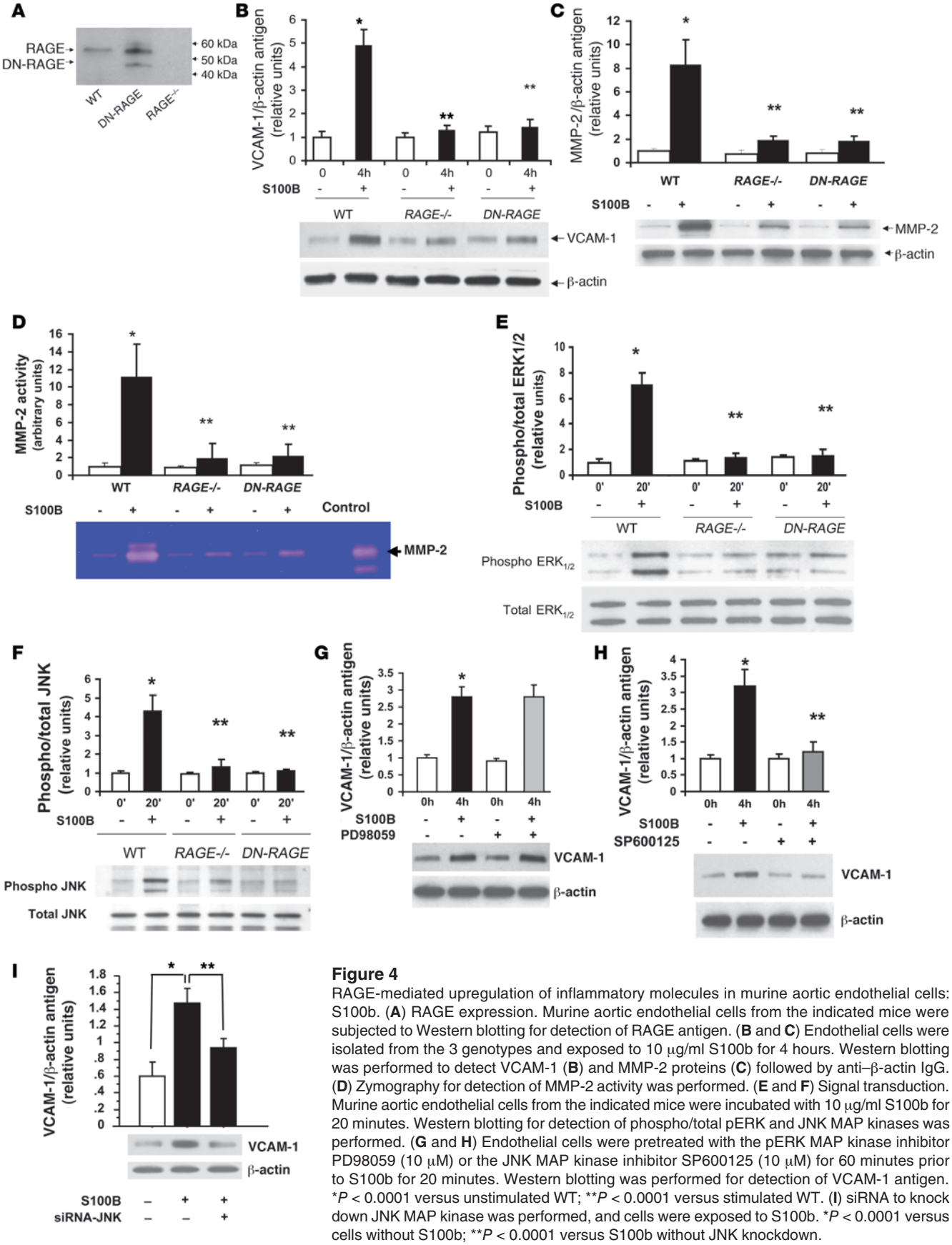

Figure 4

RAGE-mediated upregulation of inflammatory molecules in murine aortic endothelial cells: S100b. (**A**) RAGE expression. Murine aortic endothelial cells from the indicated mice were subjected to Western blotting for detection of RAGE antigen. (**B** and **C**) Endothelial cells were isolated from the 3 genotypes and exposed to 10 μg/ml S100b for 4 hours. Western blotting was performed to detect VCAM-1 (**B**) and MMP-2 proteins (**C**) followed by anti–β-actin IgG. (**D**) Zymography for detection of MMP-2 activity was performed. (**E** and **F**) Signal transduction. Murine aortic endothelial cells from the indicated mice were incubated with 10 μg/ml S100b for 20 minutes. Western blotting for detection of phospho/total pERK and JNK MAP kinases was performed. (**G** and **H**) Endothelial cells were pretreated with the pERK MAP kinase inhibitor PD98059 (10 μM) or the JNK MAP kinase inhibitor SP600125 (10 μM) for 60 minutes prior to S100b for 20 minutes. Western blotting was performed for detection of VCAM-1 antigen. *$P < 0.0001$ versus unstimulated WT; **$P < 0.0001$ versus stimulated WT. (**I**) siRNA to knock down JNK MAP kinase was performed, and cells were exposed to S100b. *$P < 0.0001$ versus cells without S100b; **$P < 0.0001$ versus S100b without JNK knockdown.

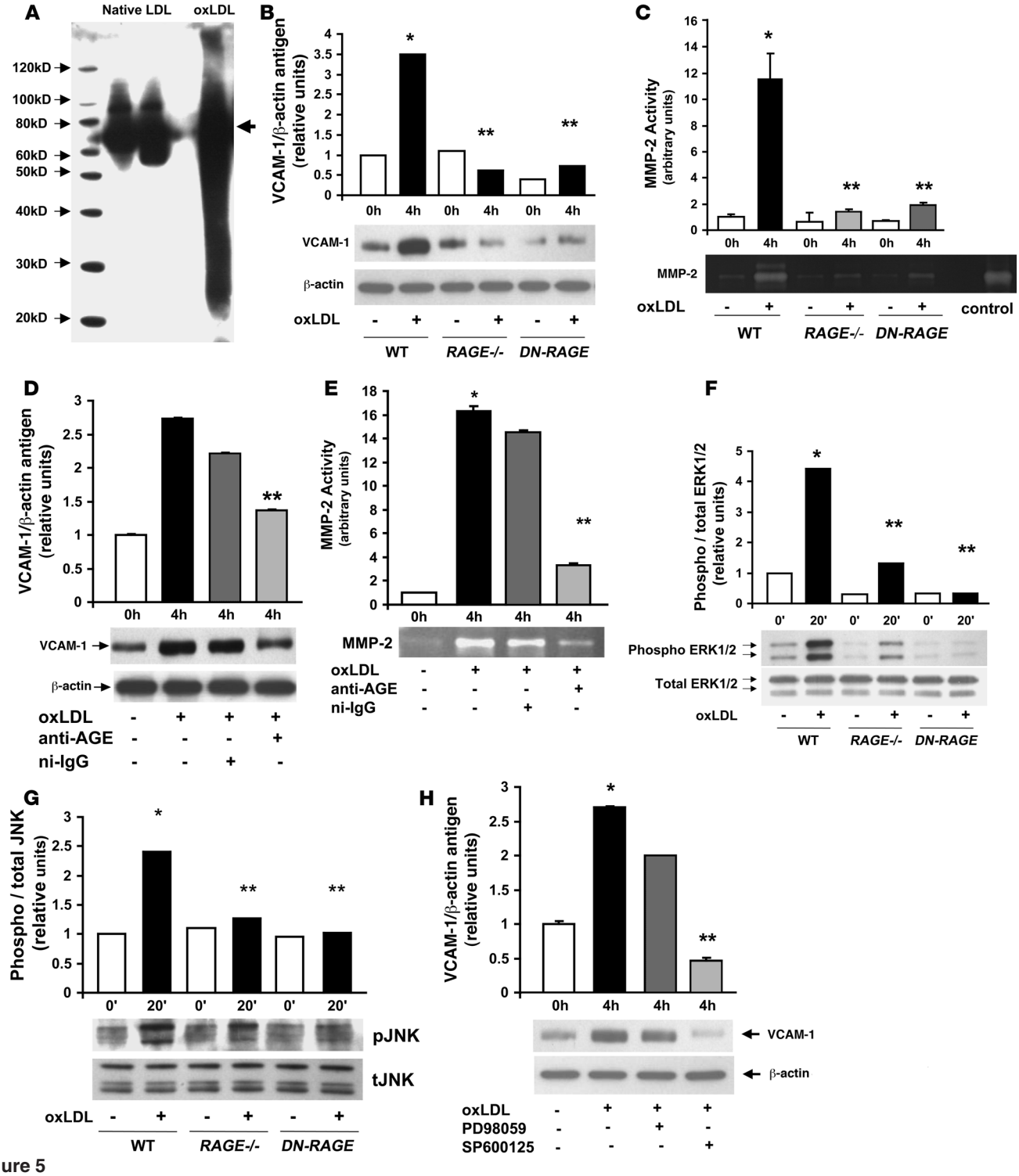

Figure 5

RAGE-mediated upregulation of inflammatory molecules in murine aortic endothelial cells: oxLDL. (**A**) oxLDL contains AGE epitopes. Native LDL and oxLDL (5 μg/ml) were subjected to SDS-PAGE and Western blotting using affinity-purified rabbit anti-AGE IgG. (**B**) Endothelial cells were incubated with 5 μg/ml oxLDL for 4 hours. Western blotting was performed for detection of VCAM-1 antigen followed by anti–β-actin IgG. (**C**) Zymography for detection of MMP-2 activity was performed. *$P < 0.0001$ versus unstimulated WT; **$P < 0.0001$ versus stimulated WT. (**D** and **E**) Effect of anti-AGE IgG. Murine aortic endothelial cells were pretreated with rabbit anti-AGE IgG or nonimmune rabbit IgG (nI-IgG; 50 μg/ml) for 1 hour. OxLDL (5 μg/ml) was added for 4 hours; cells were harvested and Western blotting was performed to detect VCAM-1 (**D**) followed by anti–β-actin IgG, or MMP-2 activity by zymography (**E**). (**F** and **G**) Signal transduction. Endothelial cells were incubated with 5 μg/ml oxLDL for 20 minutes. Western blotting for detection of phospho/total pERK and JNK MAP kinases was performed. (**H**) Endothelial cells were pretreated with the pERK MAP kinase inhibitor PD98059 (10 μM) or the JNK MAP kinase inhibitor SP600125 (10 μM) for 1 hour prior to exposure to oxLDL for 20 minutes. Western blotting was performed for detection of VCAM-1 antigen. *$P < 0.0001$ versus unstimulated WT; **$P < 0.0001$ versus oxLDL-stimulated WT.

Tg PPET DN-RAGE endothelial cells in the presence of oxLDL compared with that observed in WT endothelial cells ($P < 0.0001$; Figure 5, F and G).

We then determined the specific signaling pathways stimulated by oxLDL that accounted for upregulation of VCAM-1 antigen. WT endothelial cells were pretreated with inhibitors of either phospho-ERK or JNK MAP kinases. Compared with PD98059 pretreatment, in which no significant suppression of oxLDL-mediated upregulation of VCAM-1 was noted, pretreatment with the JNK MAP kinase inhibitor SP600125 resulted in a highly significant reduction in oxLDL-induced upregulation of VCAM-1 antigen ($P < 0.0001$; Figure 5H). Introduction of siRNA to knock down JNK expression exerted similar suppressive effects on S100b-stimulated upregulation of VCAM-1 (data not shown).

Key roles for RAGE in mediating hyperpermeability and regulation of VCAM-1 in human aortic endothelial cells. In homeostasis, the endothelium maintains a competent barrier, thereby limiting infiltration of exogenous molecules or cells. We tested the role of RAGE in mediating barrier function in human aortic endothelial cells upon exposure to RAGE ligands. Lentiviral gene transduction was used to introduce full-length RAGE (to augment RAGE expression) or DN-RAGE (to block RAGE signaling) into human endothelial cells. In the presence of S100b, a significant increase in monolayer permeability of full-length RAGE–expressing endothelial cells was noted compared with unstimulated full-length RAGE–expressing cells ($P < 0.0001$; Figure 6A). When RAGE signaling was disrupted by introduction of DN-RAGE, S100b failed to increase monolayer permeability compared with unstimulated cells bearing DN-RAGE. Furthermore, a significant difference in permeability was observed between S100b-stimulated full-length RAGE–expressing cells and S100b-stimulated DN-RAGE–expressing cells ($P < 0.0001$; Figure 6A). We next tested the role of RAGE in vascular inflammation and used siRNA to suppress RAGE expression in human aortic endothelial cells. As illustrated in Figure 6, B and C, siRNA targeted against RAGE, but not control scramble siRNA, reduced RAGE transcripts and RAGE protein.

We observed that RAGE siRNA suppressed S100b-stimulated upregulation of VCAM-1 compared with cells treated with scramble siRNA and S100b (Figure 6D). To test the possibility that JNK MAP kinase signaling mediated the effect of S100b in human endothelial cells, cells were treated with S100b. A significant time-dependent increase in phosphorylation of JNK MAP kinase was noted (about 2.5-fold that of baseline at 20 and 30 minutes of treatment; $P < 0.0001$; Figure 6E). The impact of S100b on upregulation of VCAM-1 was dependent on JNK MAP kinase signaling, as pretreatment with SP600125 significantly reduced VCAM-1 antigen ($P < 0.0001$; Figure 6F). Similarly, introduction of siRNA to knock down JNK expression in these cells suppressed S100b-stimulated upregulation of VCAM-1 (data not shown).

To extend these concepts and probe whether oxLDL-containing AGE epitopes impacted gene expression in these human endothelial cells, we first performed a time course to assess JNK MAP kinase signaling. As illustrated in Figure 6G, a time-dependent increase in phosphorylation of JNK MAP kinase was evident upon incubation with oxLDL. To examine if JNK signaling mediated upregulation of VCAM-1 by oxLDL in these cells, we used various means to block this pathway. Incubation of cells with SP600125 (Figure 6H) or introduction of siRNA to knock down JNK expression blunted oxLDL-stimulated upregulation of VCAM-1 ($P < 0.05$; Figure 6I).

Discussion

Our experiments uncovered 4 insights into roles for RAGE in vascular perturbation. First, compared with *apoE*$^{-/-}$ mice, *apoE*$^{-/-}$ *RAGE*$^{-/-}$ and *apoE*$^{-/-}$*Tg PPET DN-RAGE* mice displayed significant reduction in atherosclerosis. Second, in aortic rings retrieved from these RAGE-modified mice, significantly enhanced endothelium-dependent relaxation to acetylcholine was observed compared with *apoE*$^{-/-}$ mice. Third, in isolated endothelial cells retrieved from *RAGE*$^{-/-}$ or *Tg PPET DN-RAGE* mice, suppression of vascular inflammation and JNK signaling induced by S100b or oxLDL-containing AGE epitopes was evident. Fourth, S100b and oxLDL-containing AGEs upregulated VCAM-1 in human aortic endothelial cells, at least in part via JNK signaling.

Endothelial dysfunction and upregulation of VCAM-1, pivotal events in atherosclerosis, occur very early after lipid infiltration in the vessel; VCAM-1 expression marks the sites destined for development of atherosclerotic plaques (27). In this report, we demonstrate that RAGE mediates upregulation of VCAM-1 in the vessel wall and in murine and human aortic endothelial cells in response to S100b and oxLDL and elucidate for the first time to our knowledge that JNK MAP kinase underlies the RAGE ligand-stimulated molecular events regulating this factor in endothelial cells. Furthermore, blockade of RAGE abrogated RAGE ligand–mediated hyperpermeability in human aortic endothelial cells.

Although previous studies in cultured endothelial cells demonstrated that inflammatory signaling upregulated VCAM-1 via JNK MAP kinase (28, 29), here we demonstrate a precise ligand receptor–dependent mechanism by which these events occur. In vivo, multiple cycles of cell stimulation in the stressed vasculature sustain inflammatory signaling. For example, MCP-1, itself a target of RAGE signaling, activates MAP kinases in human endothelial cells, including ERK, JNK, and p38 pathways (30).

Our experiments in isolated endothelial cells revealed that AGE-containing epitopes within oxLDL contributed importantly to upregulation of VCAM-1 and MMP-2 activity, largely via RAGE signaling. Certainly, oxLDL-modified species display a repertoire of glycated and oxidized modification epitopes (4), yet our findings reveal roles for RAGE in stimulating signal transduction triggered by these molecules. We suggest that such events in the vessel wall prime the vasculature for consequent inflammatory stress and that RAGE contributes integrally to these processes. Specifically, we observed that proinflammatory RAGE ligands S100/calgranulins and HMGB1 were reduced in *RAGE*$^{-/-}$ and *Tg PPET DN-RAGE* mouse aortas. Possible explanations include decreased infiltration of inflammatory cells bearing these factors or enhanced ligand clearance in these mice. Studies in human subjects place S100/calgranulins and HMGB1 in atherosclerotic plaques, thereby establishing the relevance of our observations to human vascular activation (31, 32).

Our previously published experiments revealed that administration of the soluble, extracellular ligand–binding domain of RAGE suppressed atherosclerosis in predisposed mice (21, 33, 34). A caveat of those studies was that they did not provide unmitigated support that RAGE was a chief target of the ligand-binding decoy. Engagement of distinct receptors by RAGE ligands, such as scavenger receptors and TLRs (19, 20), might have accounted, at least in part, for the benefits of soluble RAGE. The finding that *apoE*$^{-/-}$ mice devoid of RAGE displayed significant suppression of atherosclerosis and vascular inflammation unequivocally establishes key roles for RAGE in atherosclerosis. Indeed, our finding

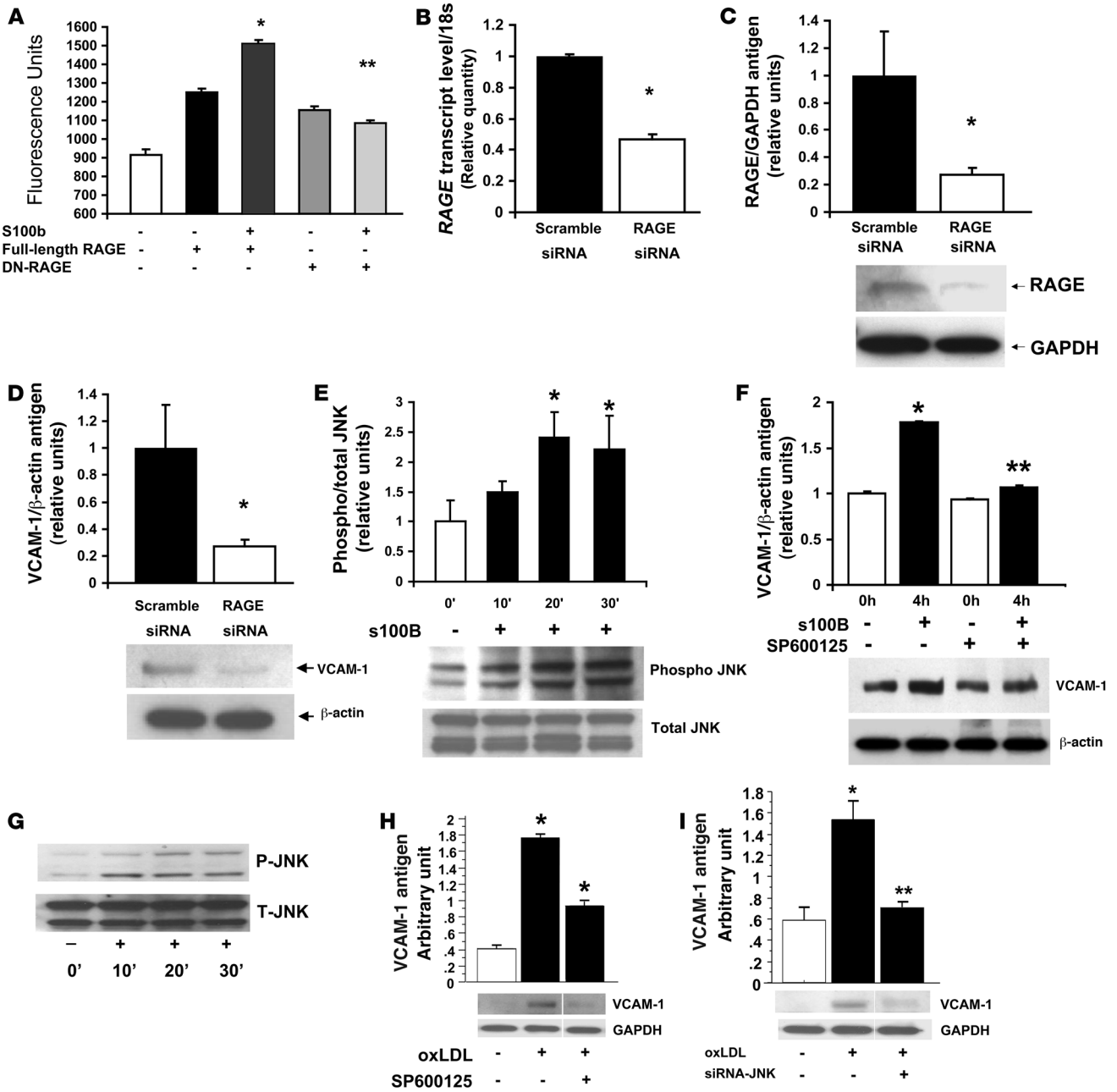

Figure 6

RAGE-mediated upregulation of inflammatory molecules in human aortic endothelial cells. (**A**) Human aortic endothelial cells were subjected to lentiviral infection introducing full-length or DN-RAGE. Cells were exposed to S100b and permeability assay performed. *$P < 0.0001$ versus unstimulated full-length RAGE; **$P < 0.0001$ versus S100b-stimulated full-length RAGE. (**B** and **C**) Human endothelial cells were subjected to introduction of siRNA to reduce RAGE transcripts (**B**) and RAGE protein (**C**) without effect on GAPDH transcripts or protein. (**D**) Endothelial cells were subjected to RAGE or scramble siRNA and incubated with 10 μg/ml S100b for 4 hours. Western blotting was performed to probe VCAM-1 antigen and β-actin. *$P < 0.0001$. (**E**) Human aortic endothelial cells were stimulated with 10 μg/ml S100b for 20 minutes. Western blotting was performed to detect phospho/total-JNK MAP kinases. *$P < 0.0001$. (**F**) Endothelial cells were treated with JNK MAP kinase inhibitor SP60025 (10 μM) for 60 minutes followed by S100b (10 μg/ml) for 4 hours and Western blotting performed with anti–VCAM-1 IgG and anti–β-actin IgG. **$P < 0.0001$ versus S100b-stimulated, non–SP600125-treated. (**G**) oxLDL (5 μg/ml) was incubated with human aortic endothelial cells and Western blotting performed for detection of phospho/total-JNK MAP kinase. (**H**) Cells were treated with 10 μM SP600125 for 1 hour followed by incubation with oxLDL for 4 hours. Western blotting was performed for detection of VCAM-1 antigen. *$P < 0.0001$. (**I**) Cells were treated with siRNA to knock down JNK MAP kinase followed by incubation with oxLDL for 4 hours. Western blotting was performed for detection of VCAM-1 antigen. Where indicated by the white line, lanes were run on the same gel but were noncontiguous. *$P < 0.05$; **$P < 0.01$.

that mRNA transcript levels of *CD36*, *TLR2*, and *TLR4* in the aorta did not differ among the 3 groups of mice further supports direct roles for RAGE in vascular signaling and atherosclerosis.

It is intriguing that *apoE*$^{-/-}$*Tg PPET DN-RAGE* mice appeared to display more overt suppression of atherosclerosis compared with the effect of RAGE deletion in vivo. However, in aortic rings and in isolated endothelial cells, the effect of either RAGE deletion or DN-RAGE was similar. It is possible that in *RAGE*$^{-/-}$ mice, potential "adaptive" roles for RAGE in nonendothelial cells such as monocytes/macrophages, T or B lymphocytes, dendritic cells, or smooth muscle cells may offset the effect of endothelial RAGE contributions to atherogenesis. Extensive experimentation has revealed both injurious and beneficial responses for innate and adaptive immune cells in atherosclerosis (35). Cells such as monocytes/macrophages, dendritic cells, and T lymphocytes, many of which express RAGE (36–39), likely play varied roles in atherosclerosis at distinct sites and time points in the disease. In this context, previous work illustrated important repair-related roles for RAGE in unilateral sciatic nerve crush in mice, at least in part via facilitation of Wallerian degeneration (40).

Lastly, it is plausible that "compensatory factors" in homozygous *RAGE*$^{-/-}$ mice may subtly shift pro- versus antiinflammatory balances in the vasculature, thereby obscuring the overall role for RAGE in vascular stress. In addition, it is possible that RAGE ligands may be diverted, in part, from non-RAGE receptors in the *Tg PPET DN-RAGE* mice.

In conclusion, our findings underscore pivotal roles for RAGE in atherosclerosis and roles for RAGE signaling in endothelial cells, as revealed by blunted S100b- and oxLDL- stimulated cellular perturbation in isolated endothelial cells from the DN-RAGE mice and in human endothelial cells bearing DN-RAGE. Taken together, our results implicate the ligand-RAGE axis in mechanisms underlying vascular and inflammatory stress in atherosclerosis in the complex milieu of the atherosclerosis-vulnerable vessel wall.

Methods

Animal studies. Homozygous *apoE*$^{-/-}$ mice were purchased from The Jackson Laboratory. Homozygous *RAGE*$^{-/-}$ mice were backcrossed more than 12 generations into C57BL/6 background. We prepared Tg mice expressing DN-RAGE in endothelial cells using the PPET-1 promoter (5.9 kb), SV40 pA and ET-1 first intron in Bluescript as a vector. DN-RAGE (1.1 kb), the 3′ end sequence deleted human RAGE cDNA (1.35 kb), was subcloned into the above vector, and Tg cassettes (8.997 kb) were created by releasing the XhoI fragments from the PPET DN-RAGE-SV40 pA-ET-1 Bluescript construct (11.181 kb). These were microinjected into mouse B6CAF1/j oocytes; the latter were implanted into pseudopregnant females, and after mating with strain-matched males, founders were identified via Southern blotting using human RAGE cDNA as a probe and by PCR using forward primer, 5′-GGAAGCCCCTGGTGCCTAATGA-3′ and reverse primer 5′-GCCCCTC-GCCTGGTTC-3′. Mice were generated and backcrossed more than 12 generations into C57BL/6. Littermates not expressing the transgene were used as controls. Mice were maintained at all times on normal rodent chow and allowed free access to food and water. Genomic DNA was isolated from tail biopsies, and PCR analysis was used to identify the deficiency of both genes (*apoE*$^{-/-}$*RAGE*$^{-/-}$) or the presence of DN-RAGE. All procedures were carried out with the approval of the Institutional Animal Care and Use Committee of Columbia University.

Biochemical analyses. Levels of total cholesterol and triglyceride were determined in plasma of fasted mice using chromogenic assays (Thermo Electron Corporation).

ELISA. At sacrifice, plasma was collected from the indicated mice, all aged 14 weeks. Concentrations of mouse soluble VCAM-1 were determined in plasma by Quantikine (R&D Systems Inc.) according to the manufacturer's instructions.

Quantification of atherosclerotic lesion area. Mice were fasted for 4 hours and then anesthetized. The aortas were harvested and stored at –80°C for Western blotting, real-time PCR, and zymography studies. The hearts were stored in acetone or 10% buffered formalin for histology studies. Six 10-μm sections were collected at 80-μm intervals starting at a 100-μm distance from the appearance of the aortic valves. Formaldehyde-fixed sections were stained with hematoxylin and oil red O. Atherosclerotic lesion areas were quantified using a Zeiss microscope and image analysis system (AxioVision 4.5). Four serial sections each were placed on 6 slides (total 24 sections), and mean lesion area was calculated by determining the mean lesion area of 1 section/slide for a total of 4 sections examined. The investigator was blinded to the experimental conditions.

Immunohistochemistry. Acetone-fixed cryostat aortic sections were preincubated with CAS-BLOCK (Zymed; Invitrogen) for 30 minutes followed by avidin-biotin block for 15 minutes; sections were then subjected to incubation with primary rabbit polyclonal RAGE IgG (2, 3) overnight at 4°C followed by goat anti-rabbit IgG (Vector Laboratories). Subsequently, Alexa Fluor 555 conjugate (Invitrogen) was incubated for 30 minutes. After washing, rat monoclonal CD31 antibody (Fitzgerald Industries) or mouse monoclonal smooth muscle actin (DakoCytomatin) antibody were incubated for 1 hour followed by anti-rat or anti-mouse IgG for 30 minutes, and then incubated with Alexa Fluor 488 conjugate for 30 minutes, finally mounted with 4,6-diamidino-2-phenylindole dihydrochloride (Vector Laboratories). Rabbit IgG (Zymed; Invitrogen) or omission of the primary antibody was used as a negative control.

Zymography. To detect MMP-2 activity, mouse aortas were homogenized, whereas cell culture media were collected and concentrated (Vivaspin; ISC Bioexpress). Electrophoresis was performed on zymogram gelatin gels (Invitrogen). After the required developing time, gels were stained with Coomasie Blue (BioRad). Images were obtained with an Alpha-Imager.

RNA isolation, cDNA synthesis, and real-time RT-PCR. Total aortic RNA was isolated from the indicated mice or cultured cells by using TRIzol (Invitrogen) and RNeasy MinElute Cleanup (QIAGEN Inc.) including a DNase step. Total RNA concentration and quality were assessed on a 2100 Bioanalyzer system (Agilent Technologies). cDNA was synthesized (TaqMan Reverse Transcription Reagents Kit; ABI) according to the manufacturer's instructions and amplified by real-time PCR on a sequence-detection system (Prism 7900HTl; ABI). Mouse *TLR2* (Mm00442346_m1), *TLR4* (Mm00445274_m1), *CD36* (Mm01135198_m1), and *RAGE* (Mn00545815 m1) probe and primers were obtained by Assay-on-demand from Applied Biosystems. We used 18s rRNA as an endogenous reference to correct for differences in the amount of RNA. Data were analyzed by the $2^{-\Delta\Delta CT}$ method. The ratio of RAGE to 18S in each sample was calculated, and the expression level of RAGE is presented relative to that of the scramble siRNA–treated cells.

Preparation of oxLDL. Human LDL (Invitrogen) was oxidized in the presence of 2.5 μmol/l $CuCl_2$ at 37°C for 48 hours and dialyzed extensively against PBS. Assessment of thiobarbituric acid reactive substances (TBARS) was used to verify the degree of oxidation (Zepto Metrix Corporation). The protein concentration of oxLDL was determined using the Lowry assay (BioRad).

Murine and human aortic endothelial cells. Mouse aortic endothelial cells were isolated from 6- to 8-week-old WT, *RAGE*$^{-/-}$, or DN-RAGE–expressing mice as described previously (41). Cells were used at identical passage numbers. All measurements were normalized to total cell protein and a housekeeping protein as indicated to control for possible differences in

cell growth. To characterize endothelial cells, we performed DiI-ac-LDL staining (Biomedical Technologies) and cord formation assay (BD Biosciences); mouse fibroblasts were used as negative control for these assays (ATCC). For all experiments cells were grown to 70%–80% confluence, serum-starved overnight, and then incubated with the indicated concentration of S100B (Calbiochem) or oxLDL for the indicated time periods. Human aortic endothelial cells were purchased from LONZA. They were grown in EGM-2 medium and used in passages 5–8. Cells were pretreated with PD98059 (Promega) or SP600125 (Sigma-Aldrich) at a final concentration of 10 μM.

siRNA to knock down expression of RAGE and JNK. siRNA duplexes against human *RAGE* were designed against the target sequence 5′-TGCCTCTGAACTCACGGCTGGTGTT-3′ and synthesized by Invitrogen. The target sequence for JNK-specific siRNA is 5′-AAAAAGAATGTCCTACCTTCT-3′ (42), which is specific for both mice and humans (43). SiRNA duplexes against *RAGE* and *JNK* were electroporated into mouse or human aortic endothelial cells using the Nucleofector device (Amaxa). To control for off-target effects of siRNA, a separate well of endothelial cells was electroporated with a scramble GC content–matched siRNA (Stealth RNAi Negative Control; Invitrogen). After 48 hours, cells were harvested for RNA isolation using TRIzol (Invitrogen) or for protein expression analysis using lysis buffer.

RAGE and DN-RAGE lentivirus construction. Full-length human RAGE (44) was generated from lung cDNA and cloned into the lentiviral expression vector pLenti6/V5-D-tOPO (Invitrogen). Human DN-RAGE was generated by PCR by inserting a stop codon into the cDNA sequence of RAGE at the end of the transmembrane domain (amino acid 361) to remove the cytoplasmic domain. Viruses were produced using the ViraPower Lentiviral Expression System (Invitrogen) according to the manufacturer's instructions. Introduction of RAGE and DN-RAGE was performed by infecting cells with multiplicity of infection of 0.5–5 and assessing RAGE expression by Western blotting as described below.

Mouse peritoneal macrophage culture. Thioglycollate-elicited macrophages were obtained from 8-week-old mice that had been injected intraperitoneally 5 days before sacrifice with 1.0 ml of a 10% solution of thioglycollate broth (Difco Laboratories Inc.) prepared according to the manufacturer's instructions. Macrophages were cultured in RPMI 1640 medium, supplemented with 10% fetal bovine serum and 1% penicillin/streptomycin for 2 days, and then subjected to serum-free medium for 24 hours before stimulating with S100B (10 μg/ml) for 20 minutes. Subsequently, the cell lysates were harvested for Western blotting as described below.

Western blot analysis. Total lysate from mouse aorta or cultured cells was used for detection of proinflammatory mediator expression with the following IgGs: VCAM-1 and CD40 (Santa Cruz Biotechnologies); MMP-2 and GAPDH (Chemicon and Abcam); IL-10 and MCP-1 (R&D Systems); S100; β-actin (Sigma-Aldrich); and HMGB-1 (BD Biosciences). Anti-RAGE IgG was purchased from R&D. Anti-phospho and anti-total ERK1/2 and JNK MAP kinase IgG were purchased from Cell Signaling Technology Inc. HRP-conjugated donkey anti-rabbit IgG or rat anti-goat secondary antibody (Amersham Pharmacia Biotechnology Inc.) were used to identify sites of binding of the primary antibody. Affinity-purified anti-AGE IgG was prepared in our laboratory (21). In all Western blot studies, at least 3 animals or cell lysates per group were used; results of representative experiments are shown.

Functional studies on isolated vessels. The investigator was blinded to genotype or treatment for all experiments, and endothelial vasorelaxation was studied as described previously (45–48). Thoracic aortas from the indicated mice were carefully excised and quickly immersed in Krebs Henseleit solution (118 mM NaCl, 5.4 mM KCl, 1.2 mM $MgCl_2$, 2.5 mM $CaCl_2$, 22 mM $NaHCO_3$, 1.2 mM NaH_2PO_4, and 10.1 mM glucose) aerated with 95% O_2 and 5% CO_2 (37°C, pH 7.4). After removal of fat and periadventitial tissue, 4 rings of 3–4 mm length were prepared from each aorta and were mounted in 20-ml organ bath chambers (Experimentria) filled with Krebs Henseleit solution (37°C, pH 7.4) using 2 tungsten wire triangles. A passive tension (preload) of 0.75 g was applied in each ring. After equilibration and preconditioning, cumulative concentration-response curves to acetylcholine (10^{-8} to 10^{-4} M) were obtained in rings precontracted with 1 maximal dose of phenylephrine (10^{-6} M) that produced submaximal contraction. Changes in isometric tension were recorded by a force transducer (Experimentria) connected to a tissue force analyzer. The relaxant effect to each acetylcholine dose was expressed as percentage vasorelaxation relative to the initial phenylephrine precontraction.

Cell permeability assay. An in vitro endothelial cell permeability assay (Chemicon) was performed as follows: 3×10^4 human aortic endothelial cells were seeded into inserts in a 24-well tissue culture dish. After growth of cells to a monolayer, RAGE or DN-RAGE lentivirus infection was performed and cells were allowed to grow for 24 hours followed by overnight starvation. RAGE ligand S100b was added to the upper chamber, and cellular permeability was induced during the overnight period. Control wells with no stimulation were included. FITC-Dextran solution was added for 5 minutes to the upper chamber, and the extent of permeability of the monolayer was determined by measuring the fluorescence of the lower plate well solution using the CytoFluor fluorescent plate reader (Applied Biosystems).

Statistics. In all experiments, unless otherwise indicated, data are reported as mean ± SEM in at least 3 replicates per group. For studies in aortic rings, percentages of vasodilation in response to each concentration of agonist were compared in different 2-way ANOVA tests using Student Newman-Keuls pairwise comparisons in order to determine the effect of RAGE mutation on endothelium-dependent vasodilation. For all other studies, data were analyzed by ANOVA and, as indicated, subjected to post-hoc comparisons using 2-tailed *t* test. A *P* value less than 0.05 was considered significant.

Acknowledgments

The authors gratefully acknowledge grant support provided by the U.S. Public Health Service and the Juvenile Diabetes Research Foundation. We are grateful to Latoya Woods for her expertise in preparation of the manuscript. We are grateful to Catherine Hedrick, Suseela Srinivasan, and colleagues at the University of Virginia in whose laboratory we learned techniques to isolate and characterize primary murine aortic endothelial cells.

Received for publication May 16, 2007, and accepted in revised form October 24, 2007.

Address correspondence to: Ann Marie Schmidt, Division of Surgical Science, Department of Surgery, Columbia University Medical Center, 630 West 168th Street, P&S 17-501, New York, New York 10032, USA. Phone: (212) 305-6406; Fax: (212) 305-5337; E-mail: ams11@columbia.edu.

Shi Fang Yan and Ann Marie Schmidt are co-senior authors.

1. Kislinger, T.K., et al. 1999. N(epsilon)-(carboxymethyl)lysine adducts of proteins are ligands for receptor for advanced glycation end products that activate cell signaling pathways and modulate gene expression. *J. Biol. Chem.* **274**:31740–31749.
2. Hofmann, M.A., et al. 1999. RAGE mediates a novel proinflammatory axis: a central cell surface receptor for S100/calgranulin polypeptides. *Cell.* **97**:889–901.
3. Taguchi, A., et al. 2000. Blockade of RAGE-amphoterin signalling suppresses tumour growth and metastases. *Nature.* **405**:354–360.
4. Imanaga, Y., et al. 2000. In vivo and in vitro evidence for the glycoxidation of low density lipoprotein in human atherosclerotic plaques. *Atherosclerosis.*

150:343–355.
5. Cybulsky, M.I., and Gimbrone, M.A. 1991. Endothelial expression of a mononuclear leukocyte adhesion molecule during atherosclerosis. *Science.* **251**:788–791.
6. Rajavashisth, T.B., et al. 1990. Induction of endothelial cell expression of granulocyte and macrophage colony-stimulating factors by modified low-density lipoproteins. *Nature.* **344**:254–257.
7. Boring, L., Gosling, J., Cleary, M., and Charo, I.F. 1998. Decreased lesion formation in CCR2$^{-/-}$ mice reveals a role for chemokines in the initiation of atherosclerosis. *Nature.* **394**:894–897.
8. Gu, L., et al. 1998. Absence of monocyte chemoattractant protein–1 reduces atherosclerosis in low density lipoprotein receptor–deficient mice. *Mol. Cell.* **2**:275–281.
9. Rammes, A., et al. 1997. Myeloid-related protein (MRP) 8 and MRP14, calcium-binding proteins of the S100 family, are secreted by activated monocytes via a novel, tubulin-dependent pathway. *J. Biol. Chem.* **272**:9496–9502.
10. Wang, H., et al. 1999. HMG-1 as a late mediator of endotoxin lethality in mice. *Science.* **285**:248–251.
11. Asahi, K., et al. 2000. Nitric oxide inhibits the formation of advanced glycation endproducts. *Kidney Int.* **58**:1780–1787.
12. Anderson, M.M., and Heinecke, J.W. 2003. Production of N(epsilon)-(carboxymethyl)lysine is impaired in mice deficient in NADPH oxidase: a role for phagocyte-derived oxidants in the formation of advanced glycation endproducts during inflammation. *Diabetes.* **52**:2137–2143.
13. Sakaguchi, T., et al. 2003. Central role of RAGE-dependent neointimal expansion in arterial restenosis. *J. Clin. Invest.* **111**:959–972.
14. Plump, A.S., et al. 1992. Severe hypercholesterolemia and atherosclerosis in apolipoprotein E-deficient mice created by homologous recombination in ES cells. *Cell.* **71**:343–353.
15. Piedrahita, J.A., Zhang, S.H., Hagaman, J.R., Oliver, P.M., and Maeda, N. 1992. Generation of mice carrying a mutant apolipoprotein E gene inactivated by gene targeting in embryonic stem cells. *Proc. Natl. Acad. Sci. U. S. A.* **89**:4471–4475.
16. Yonekura, H., et al. 2003. Novel splice variants of the receptor for advanced glycation end-products expressed in human vascular endothelial cells and pericytes, and their putative roles in diabetes-induced vascular injury. *Biochem. J.* **370**:1097–1109.
17. Srikrishna, G., et al. 2002. N-glycans on the receptor for advanced glycation end products influence amphoterin binding and neurite outgrowth. *J. Neurochem.* **80**:998–1008.
18. Harats, D., et al. 1995. Targeting gene expression of the vascular wall in transgenic mice using the murine preproendothelin-1 promoter. *J. Clin. Invest.* **95**:1335–1344.
19. Ohgami, N., et al. 2002. CD36 serves as a receptor for advanced glycation endproducts. *J. Diabetes Complicat.* **16**:56–59.
20. Park, J.S., et al. 2004. Involvement of toll-like receptors 2 and 4 in cellular activation by high mobility group box 1 protein. *J. Biol. Chem.* **279**:7370–7377.
21. Park, L., et al. 1998. Suppression of accelerated diabetic atherosclerosis by soluble Receptor for AGE (sRAGE). *Nat. Med.* **4**:1025–1031.
22. Vincent, L., et al. 2001. Inhibition of endothelial cell migration by cerivastatin, an HMG-CoA reductase inhibitor: contribution to its anti-angiogenic effect. *FEBS Lett.* **495**:159–166.
23. Park, H.Y., et al. 2001. Potential role of leptin in angiogenesis: leptin induces endothelial cell proliferation and expression of matrix metalloproteinases in vivo and in vitro. *Exp. Mol. Med.* **33**:95–102.
24. Mallat, Z., et al. 1999. Protective role of interleukin-10 in atherosclerosis. *Circ. Res.* **85**:e17–e24.
25. Mach, F., Schoenbeck, U., Bonnefoy, J.Y., Pober, J., and Libby, P. 1997. Activation of monocyte/macrophage functions related to acute atheroma complication by ligation of CD40. Induction of collagenase, stromelysin, and tissue factor. *Circulation.* **96**:396–399.
26. Mach, F., Schonbeck, U., Sukhova, G.K., Atkinson, E., and Libby, P. 1998. Reduction of atherosclerosis in mice by inhibition of CD40 signaling. *Nature.* **394**:200–203.
27. Nakashima, Y., Raines, E.W., Plump, A.S., Breslow, J.L., and Ross, R. 1998. Upregulation of VCAM–1 and ICAM–1 at atherosclerosis–prone sites on the endothelium in the apoE–deficient mouse. *Arterioscler. Thromb. Vasc. Biol.* **18**:842–851.
28. Yoshizumi, M., et al. 2004. Ebselen inhibits tumor necrosis factor alpha induced c-Jun N-terminal kinase activation and adhesion molecule expression in endothelial cells. *Exp. Cell Res.* **292**:1–10.
29. Lin, S.J., et al. 2005. Superoxide dismutase inhibits the expression of vascular cell adhesion molecule-1 and intracellular adhesion molecule-1 induced by tumor necrosis factor alpha in human endothelial cells through the JNK/p38 pathways. *Arterioscler. Thromb. Vasc. Biol.* **25**:334–340.
30. Werle, M., Schmal, U., Hanna, K., and Kreuzer, J. 2002. MCP-1 induces activation of MAP-kinases ERK,JNK and p38 MAPK in human endothelial cells. *Cardiovasc. Res.* **56**:284–292.
31. Bobryshev, Y.V., and Lord, R.S. 1995. S-100 positive cells in human arterial intima and in atherosclerotic lesions. *Cardiovasc. Res.* **29**:689–696.
32. Kalinina, N., et al. 2004. Increased expression of DNA-binding cytokine HMGB1 in human atherosclerotic lesions: role of activated macrophages and cytokines. *Arterioscler. Thromb. Vasc. Biol.* **24**:2320–2325.
33. Bucciarelli, L.G., et al. 2002. RAGE blockade stabilizes established atherosclerosis in diabetic apolipoprotein E null mice. *Circulation.* **106**:2827–2835.
34. Wendt, T., et al. 2006. RAGE modulates vascular inflammation and atherosclerosis in a murine model of type 2 diabetes. *Atherosclerosis.* **185**:70–77.
35. Hansson, G.K., and Libby, P. 2006. The immune response in atherosclerosis: a double-edged sword. *Nat. Rev. Immunol.* **6**:508–519.
36. Yan, S.S., et al. 2003. Suppression of experimental autoimmune encephalomyelitis by selective blockade of encephalitogenic T-cell infiltration of the central nervous system. *Nat. Med.* **9**:287–293.
37. Chen, Y., et al. 2004. Blockade of late stages of autoimmune diabetes by inhibition of the receptor for advanced glycation end products. *J. Immunol.* **173**:1399–1405.
38. Dumitriu, I.E., et al. 2005. Release of high mobility group box 1 by dendritic cells controls T cell activation via the receptor for advanced glycation end products. *J. Immunol.* **174**:7506–7515.
39. Cataldegirmen, G., et al. 2005. RAGE limits regeneration after massive liver injury by coordinated suppression of TNF–alpha and NF–kappaB. *J. Exp. Med.* **201**:473–484.
40. Rong, L.L., et al. 2004. RAGE modulates peripheral nerve regeneration via recruitment of both inflammatory and axonal outgrowth pathways. *FASEB J.* **18**:1818–1825.
41. Srinivasan, S., et al. 2003. Glucose regulates monocyte adhesion through endothelial production of interleukin-8. *Circ. Res.* **92**:371–377.
42. Gururajan, M., et al. 2005. C-Jun N-terminal kinase (JNK) is required for survival and proliferation of B-lymphoma cells. *Blood.* **106**:1382–1391.
43. Li, G., Xiang, Y., Sabapathy, K., and Silverman, R.H. 2004. An apoptotic signaling pathway in the interferon antiviral response mediated by RNase L and c-Jun NH_2^- terminal kinase. *J. Biol. Chem.* **279**:1123–1131.
44. Neeper, M., et al. 1992. Cloning and expression of a cell surface receptor for advanced glycosylation end products of proteins. *J. Biol. Chem.* **267**:14998–15004.
45. d'Uscio, L.V., et al. 2001. Mechanism of endothelial dysfunction in apolipoprotein E deficient mice. *Arterioscler. Thromb. Vasc. Biol.* **21**:1017–1022.
46. Ohashi, M., Runge, M.S., Faraci, F.M., and Heistad, D.D. 2006. MnSOD deficiency increases endothelial dysfunction in apoE-deficient mice. *Arterioscler. Thromb. Vasc. Biol.* **26**:2331–2336.
47. Laursen, J.B., et al. 2001. Endothelial regulation of vasomotion in apoE-deficient mice: implications for interactions between peroxynitrite and tetrahydrobiopterin. *Circulation.* **103**:1282–1288.
48. Villeneuve, N., et al. 2003. Persistence of the nitric oxide pathway in the aorta of hypercholesterolemic apolipoprotein-E-deficient mice. *J. Vasc. Res.* **40**:87–96.